frontiers | Frontiers in Immunology

TYPE Original Research
PUBLISHED 06 October 2022
DOI 10.3389/fimmu.2022.949299

OPEN ACCESS

EDITED BY
Vijayakumar Velu,
Emory University, United States

REVIEWED BY
Victor C. Huber,
University of South Dakota, United States
David J. Topham,
University of Rochester, United States

*CORRESPONDENCE
Malin Eriksson
malin.eriksson.2@ki.se

SPECIALTY SECTION
This article was submitted to Viral Immunology, a section of the journal Frontiers in Immunology

RECEIVED 20 May 2022
ACCEPTED 23 September 2022
PUBLISHED 06 October 2022

CITATION
Eriksson M, Nylén S and Grönvik K-O (2022) T cell kinetics reveal expansion of distinct lung T cell subsets in acute versus in resolved influenza virus infection.
Front. Immunol. 13:949299.
doi: 10.3389/fimmu.2022.949299

T cell kinetics reveal expansion of distinct lung T cell subsets in acute versus in resolved influenza virus infection

Malin Eriksson[1,2]*, Susanne Nylén[1] and Kjell-Olov Grönvik[3]

[1]Department of Microbiology, Tumor and Cell Biology, Karolinska Institutet, Stockholm, Sweden, [2]Department of Microbiology, National Veterinary Institute, Uppsala, Sweden, [3]Uppsala Immunobiology Lab, Uppsala, Sweden

Influenza virus infection is restricted to airway-associated tissues and elicits both cellular and humoral responses ultimately resulting in generation of memory cells able to initiate a rapid immune response against re-infections. Resident memory T cells confer protection at the site of infection where lung-resident memory T cells are important for protecting the host against homologous and heterologous influenza virus infections. Mapping kinetics of local and systemic T cell memory formation is needed to better understand the role different T cells have in viral control and protection. After infecting BALB/c mice with influenza virus strain A/Puerto Rico/8/1934 H1N1 the main proportion of activated T cells and B cells expressing the early activation marker CD69 was detected in lungs and lung-draining mediastinal lymph nodes. Increased frequencies of activated cells were also observed in the peripheral lymphoid organs spleen, inguinal lymph nodes and mesenteric lymph nodes. Likewise, antigen-specific T cells were most abundant in lungs and mediastinal lymph nodes but present in all organs studied. $CD8^+CD103^-CD49a^+$ lung-resident T cells expanded simultaneously with timing of viral clearance whereas $CD8^+CD103^+CD49a^+$ lung-resident T cells was the most abundant subset after resolution of infection and antigen-specific, lung-resident T cells were detected up to seven months after infection. In conclusion, the results in this detailed kinetic study demonstrate that influenza virus infection elicits adaptive immune responses mainly in respiratory tract-associated tissues and that distinct subsets of lung-resident T cells expand at different time points during infection. These findings contribute to the understanding of the adaptive immune response locally and systemically following influenza virus infection and call for further studies on the roles of the lung-resident T cell subsets.

KEYWORDS

influenza virus, resident T cells, Trm, CD69, CD103, CD49a

Introduction

Despite existing vaccines and extensive research, influenza virus continues to pose a global health threat and approximately 291000 – 645000 human influenza A virus-related respiratory deaths are estimated to occur annually (1). The infection is normally restricted to the respiratory tract resulting in symptoms including cough, fatigue, fever and malaise (2, 3). After viral entry, the surface glycoprotein hemagglutinin binds to α2,3-linked sialic acid receptors on ciliated airway epithelial cells (4). Once inside the epithelial cell, the virus uses the host machinery to produce viral progeny which is released from the cell, a process facilitated by the other influenza virus surface glycoprotein neuraminidase (5). Dendritic cells (DCs) in the lungs acquire influenza virus antigens from infected airway epithelial cells or by direct infection of the DCs (6–8). The DCs then migrate to lung-draining mediastinal lymph nodes (MLNs) and to spleen *via* afferent lymphatic vessels where they prime $CD4^+$ and $CD8^+$ T cells 2 – 3 days *post* infection (dpi) by establishing stable contacts resulting in activation of antigen-specific T cells (9–14). CD69 is expressed within hours after engagement of the antigen-binding receptor with its cognate antigen and is used as a marker of early activation of T cells, B cells and NK cells (15–17). After up to 48 hours of interaction with DCs the T cells detach from the DCs, start their clonal expansion but remain in the MLNs for another 48 hours before migrating to the lungs (9, 10). Natural infection with influenza virus elicits both B and T cell responses with subsequent development of humoral and cellular immunity after viral clearance (14). Unlike B cells, T cells recognize conserved influenza virus epitopes thus providing protection against heterosubtypic infections as well as potential protection against antigenic drift variants (18). Antigen-specific effector and memory T cells express CD44, indicative of antigen-experience, and populate lymphoid and non-lymphoid organs throughout the body (19–22). In contrast to CD69, CD44 is upregulated on T cells within days after activation (23).

Tissue-resident memory T cells (Trm) constitute heterogenous populations located in various tissues throughout the body e.g. skin, intestines, salivary glands and lungs (24, 25). Trm in the lungs are assigned to be of particular importance for conveying heterosubtypic immunity and provide local protection against invading pathogens by e.g. clearing influenza virus 36 – 48 hours faster after re-infection (18, 26). Both $CD4^+$ and $CD8^+$ Trm are established after influenza virus infection in mice and based on various surface markers different subsets can be distinguished (26–28). The following three subsets of $CD8^+CD69^+$ lung-resident memory T cells have been described based on surface expression of integrins CD49a and CD103: $CD103^+CD49a^-$ epithelial effector Trm (eeTrm), $CD103^+CD49a^+$ epithelial Trm (eTrm) and $CD103^-CD49a^+$ interstitial Trm (iTrm) (28). The subsets are proposed to reside at different locations in the lung tissue with iTrm in the interstitium, eeTrm within the respiratory epithelium and eTrm in the respiratory epithelium in contact with the basement membrane (28). All subsets have effector functions including production of antiviral cytokines with $CD103^+CD49a^+$ Trm expressing the highest level and $CD103^+CD49a^-$ Trm the lowest level (29). Duration of local protection against heterosubtypic challenge is reported to decline at 15 weeks *post* priming and is depleted 4 – 5 months *post* immunization (18). In comparison, influenza virus-specific T cells in the spleen remain at least for two years after infection (30).

Apart from the lung-draining lymph nodes, priming of T cells occurs in the spleen after influenza virus infection. However, little is known about priming of T cells in other lymphoid organs and in this study, we sought to investigate whether an immune response against influenza virus was elicited in secondary lymphoid organs not draining the site of infection and its kinetics. Furthermore, the kinetics of different pulmonary Trm subsets after influenza virus infection has not been studied previously. Therefore, we performed a kinetic study of the B cell and T cell responses in lungs and lung-draining MLNs as well as in spleen, inguinal lymph nodes (ILNs) and mesenteric lymph nodes (MesLNs). We demonstrate that activation of the adaptive immune response with subsequent differentiation of antigen-specific effector memory T cells (Tem) occurs in lungs and MLNs and to a minor extent in the other organs studied. Furthermore, expansion of lung-resident $CD8^+CD103^-CD49a^+$ T cells was observed simultaneously with viral clearance whereas $CD103^+CD49a^+$ T cells was the dominating subset early after resolution of infection but both subsets remained at 7 months *post* infection, and we therefore hypothesize on the biological significance of these findings.

Materials and methods

Mice and influenza virus infection

Female BALB/cAnNCrl mice aged 5 – 9 weeks bred and maintained under specific pathogen-free conditions at the animal facility of the National Veterinary Institute (SVA), Uppsala, Sweden were used. The mice were housed in groups of up to eight mice under climate-controlled conditions with a 12h:12h light-dark cycle in open-top conventional EU type 3 cages (dimensions 425 mm x 276 mm x 153 mm, floor area 820 cm^2, Tecniplast) and fed R3 (Lantmännen, Stockholm, Sweden) and/or RM3A (P) (SDS, Essex, United Kingdom) *ad libitum*. The mice were infected intranasally with 2.5 x 10^4 $TCID_{50}$ influenza virus (strain A/Puerto Rico/8/1934 H1N1) (PR8) cultured in-house or with 2 x 10^3 $TCID_{50}$ PR8 purchased from Charles River (Charles River Laboratories, RRID : SCR_003792) in 25 µl PBS under light isoflurane anesthesia. The in-house PR8 was generated and purity confirmed as previously described

(31). All animal experimental procedures were in accordance with EU directive 2010/63/EU and approved by the regional animal ethics committee of Uppsala, Sweden.

In vivo treatment with anti-CD45.2 antibodies

200 µl PBS (SVA, Uppsala, Sweden) with 3 µg of FITC-conjugated antibodies against the alloantigen CD45.2, present on the majority of hematopoietic cells, was injected intravenously in the lateral tail vein of mice three minutes prior to euthanasia according to the protocol elaborated by Andersson et al. (32). Splenic cells and peripheral blood leucocytes were analyzed as controls of successful staining.

Flow cytometry

At 1 – 210 days *post* infection the mice were euthanized by cervical dislocation and MLNs, lungs, spleens, ILNs and MesLNs were collected in 10 ml PBS (SVA, Uppsala, Sweden). Single-cell suspensions were prepared by passage through a metal mesh followed by repeated passages through a 23-gauge needle. To remove red blood cells, MLN, lung and splenic cells were lysed with ammonium-chloride-potassium (ACK) lysing buffer (SVA, Uppsala, Sweden) for 1 – 2 minutes and suspended in FACS buffer (PBS + 1% fetal calf serum). The number of viable cells were determined using Trypan blue (SVA, Uppsala, Sweden) exclusion test. The cells were stained for 30 minutes at +4°C with the following monoclonal antibodies diluted 1:50 in FACS buffer: PerCP hamster anti-mouse CD3e (145-2C11) (BD Biosciences Cat# 553067, RRID : AB_394599), V500 rat anti-mouse CD4 (RM4-5) (BD Biosciences Cat# 560782, RRID : AB_1937315)/FITC rat anti-mouse CD4 (GK1.5) (BD Biosciences Cat# 553729, RRID : AB_395013), APC rat anti-mouse CD8α (53-6.7) (BD Biosciences Cat# 553035, RRID : AB_398527), BV510 rat anti-mouse CD8α (53-6.7) (BD Biosciences Cat# 563068, RRID : AB_2687548), FITC rat anti-mouse CD8α (53-6.7) (BD Biosciences Cat# 553031, RRID : AB_394569), PE rat anti-mouse CD44 (IM7) (BD Biosciences Cat# 553134, RRID : AB_394649), FITC rat-anti mouse CD44 (IM7) (BD Biosciences Cat# 553133, RRID : AB_2076224), APC rat anti-mouse CD62L (MEL-14) (BD Biosciences Cat# 553152, RRID : AB_398533), APC-Cy7 rat anti-mouse CD62L (MEL-14) (BD Biosciences Cat# 560514, RRID : AB_10611861), V450 rat anti-mouse CD19 (1D3) (BD Biosciences Cat# 560375, RRID : AB_1645269), BV510 rat anti-mouse CD103 (M290) (BD Biosciences Cat# 563087, RRID : AB_2721775), PerCP-Cy5.5 hamster anti-rat/mouse CD49a (Ha31/8) (BD Biosciences Cat# 564862, RRID : AB_2734135), PerCP-Cy5.5 rat anti-mouse CD11a (2D7) (BD Biosciences Cat# 562809, RRID : AB_2737809), and PE-Cy7 hamster anti-mouse CD69 (H1.2F3) (BD Biosciences Cat# 552879, RRID : AB_394508), all from BD Biosciences (BD Biosciences, RRID : SCR_013311). To block unspecific binding purified rat anti-mouse CD16/CD32 (2.4G2) (BD Biosciences Cat# 553142, RRID : AB_394657) diluted 1:50, was added. For detection of antigen-specific T cells the cells were stained with tetramers before surface staining. The following reagents were obtained through the NIH Tetramer Core Facility: H-2K(d) influenza A $NP_{147-155}$, I-A(d) influenza A M_{2-17} tetramers and CLIP peptide-containing negative controls conjugated to BV421 and APC. For tetramer and CLIP-peptide containing controls, cells were stained with 4 µg/ml tetramer/CLIP in high-glucose DMEM supplemented with pyruvate, GlutaMAX™ and 2% fetal calf serum (Gibco) at +37.5°C for 75 minutes. After staining the cells were washed once, suspended in FACS-buffer and acquired on a BD FACSVerse™ and analyzed with FlowJo (FlowJo, RRID : SCR_008520) version 10. Fluorescence minus one (FMO) controls were used for gating. Gating strategy for activated T and B cells, CD44hi and Tem is shown in Figure 1 in (Table 1 in Supplementary Material).

Detection of viral RNA

Tissue specimens for PCR were taken from bone marrow, MLNs, lungs, ILNs, and spleen from mice infected intranasally with 10^4 or 10^6 $TCID_{50}$ PR8 two days earlier. The qualitative determination of H1N1 PR8 influenza virus nucleic acid in the tissues was performed by the molecular diagnostic laboratory at the National Veterinary Institute, Uppsala, Sweden using an AgPath-ID one-step real-time transcriptase PCR (RT-PCR) kit (Applied Biosystems). Tissue samples were homogenized in a Tissue Lyser (Qiagen), and extraction of virus nucleic acid was done with Nordiag Magnatrix 8000+ extraction robot using a Viral NA kit (Nordiag). The following PCR primers were used: PaninflAForward, GGGTAGATAATCACTCACTGAGTG, PaninflAReverse, CTCTGATYTCAGTNGCATTCTG, and pan-influenza virus NP, 6-FAM–ATGGCGTCTCAAGGCAC CAAACG–BHQ-1 (fluorescence-labeled probe with black hole quencher). Positive virus controls and negative Tris-EDTA (TE) buffer (SVA, Uppsala, Sweden) controls were used in the real-time RT-PCR.

Statistical analysis

GraphPad Prism (GraphPad Prism, RRID : SCR_002798) version 9 was used to prepare the graphs and perform the statistical analysis. To test whether frequencies and cell numbers after infection were statistically significant from those of naïve mice, one-way ANOVA followed by Tukey's multiple comparisons test were performed. When variances of the populations were significantly different as determined by

Bartlett's test and Brown-Forsythe test the latter and Welch ANOVA tests were performed followed by Dunnett's T3 multiple comparisons test. Data is shown as mean ± standard error of the mean (SEM) and stars indicate a statistically significant difference when compared with values obtained from uninfected mice (0 dpi). The following was used to denote statistical significance * = p< 0.05, ** = p< 0.01, *** = p< 0.001 and **** = p< 0.0001.

Results

Influenza virus infection results in activation of T cells and B cells in respiratory tract-associated tissues and peripheral lymphoid organs

To test the spread of the virus in lymphoid tissues and in lungs, groups of three BALB/c mice were infected intranasally with a sublethal dose or a lethal dose of PR8. At 48 hours *post* infection the Ct values indicated significant presence of viral RNA in a dose-dependent manner in MLNs and in lungs. No viral RNA was detected in spleen, ILNs or in bone marrow (Table 1 in Supplementary Material). Thus, the intranasal administration route mimics a natural infection *via* the upper airways where influenza virus is contained within susceptible tissues of the respiratory tract.

To study the adaptive immune response after influenza virus infection mice were infected intranasally with PR8 and euthanized at indicated time points up to 7 months *post* infection. The cardinal symptom is a dose-dependent transient weight loss which reaches its maximum at 7 – 10 dpi (Figure 1A) (3, 33). A first wave of cell accumulation was observed in lungs and lung-draining MLNs at 3 dpi followed by a second wave at 6 and 8 dpi in MLNs and lungs respectively (Figure 1B). In previous reports it was found that pulmonary inflammation persists at least three weeks after influenza virus infection which is in line with our finding that total cell numbers in MLNs and lungs were still increased at 29 dpi but had returned to baseline levels at seven months *post* infection (34). However, cell numbers in ILNs were significantly reduced days 8 and 12 *post* infection, possibly reflecting a migration of cells to the site of infection (Figure 1C). Using flow cytometry cell surface expression of the early activation marker CD69 was analyzed in T cells and in B cells. The infection triggered activation of both helper and cytotoxic T cells in MLNs, lungs, spleen and ILNs

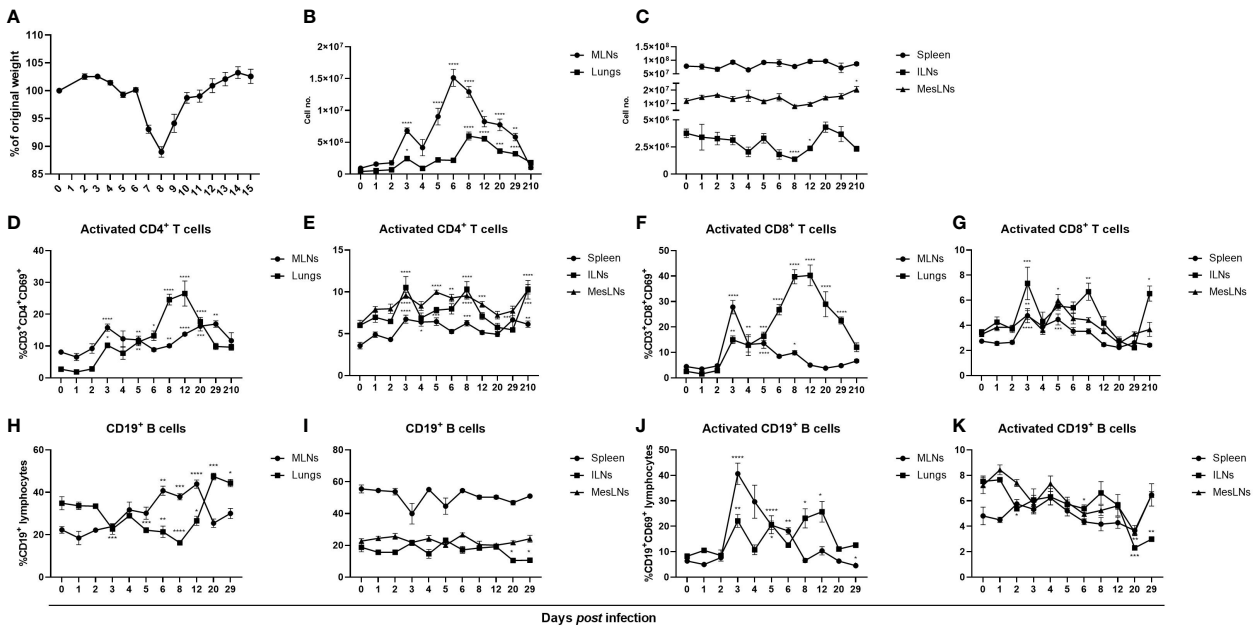

FIGURE 1
Influenza virus infection in mice results in a transient weight loss and activation and proliferation of B cells and T cells primarily in airway-associated tissues. BALB/c females aged 4 – 9 weeks old were infected with the mouse adapted H1N1 influenza A virus PR8 and monitored daily for changes in weight **(A)**. At indicated time points the mice were euthanized followed by collection of MLNs, lungs, spleen, ILNs and MesLNs and viable cells in single-cell suspensions were counted using trypan blue exclusion test **(B, C)** and analyzed with flow cytometry. Frequencies of activated helper T cells and cytotoxic T cells gated on $CD3^+$ lymphocytes in MLNs, lungs **(D, F)**, spleen, ILNs and MesLNs **(E, G)**. Frequencies of $CD19^+$ B cells gated on total lymphocytes **(H, I)** and activated $CD19^+$ B cells **(J, K).** Data in A is representative weight data from one separate experiment. Data in figures B – K are composites of 1 – 4 separate experiments per time point with 3 – 10 mice per group. Data are shown as mean ± SEM. *p < 0.05, **p < 0.01, ***p < 0.001 and ****p < 0.0001.

with the highest frequencies observed in MLNs and lungs (Figures 1D–G). In MLNs, lungs and spleen the numbers of activated T cells reflected the increased frequencies (Figure 2 in Supplementary Material). In MLNs, a biphasic activation of T helper cells was observed whereas in lungs the proportion of CD69-expressing T cells continued to increase until 12 dpi (Figure 1D). At seven months *post* infection the frequencies of CD69-expressing T helper cells in spleen, ILNs and MesLNs and cytotoxic T cells in ILNs were slightly increased (Figures 1E, G). The frequency of $CD19^+$ B cells decreased in lungs 5 – 8 dpi with the corresponding increase in MLNs that lasted until 12 dpi (Figure 1H). After 8 dpi the proportion of $CD19^+$ B cells increased in lungs and remained increased until 29 dpi (Figure 1H). The proportion of $CD19^+$ B cells returned to baseline in MLNs by day 20 *post* infection (Figure 1H). In spleen and ILNs a minor decrease in frequencies, but not numbers, of $CD19^+$ B cells occurred at 20 and 29 dpi whereas the frequency remained unaltered in MesLNs (Figure 1I, Figure 2 in Supplementary Material). Activated $CD19^+$ B cells increased substantially at 3 dpi and decreased until 12 dpi in MLNs but in lungs a minor increase in frequency was observed at 3 dpi and then a second increase was observed at 8 – 12 dpi (Figure 1J) whereas the frequencies decreased in MesLNs at 6, 8 and 20 dpi; and 2 and 29 dpi in ILNs (Figure 1K). The results demonstrate that influenza virus infection activates the adaptive immune response in lungs and lung-draining MLNs to a higher degree than in the peripheral lymphoid organs spleen, ILNs and MesLNs.

Differentiation of antigen-specific T cells occurs locally at the site of infection and systemically after influenza virus infection

Formation of effector cells in lungs after influenza virus infection has previously been demonstrated (33). Since an increase of activated T cells was observed in peripheral lymphoid organs not directly involved in the infection, we investigated whether antigen-specific effector T cells were also present. As enhanced frequencies of CD44-expressing T cells were observed in all organs investigated, apart from $CD8^+CD44^{hi}$ T cells in ILNs, at 29 dpi (Figures 2A–D) anti-CD62L antibodies were added to discriminate Tem ($CD44^{hi}$ $CD62L^{low}$) from central memory T cells ($CD44^{hi}$ $CD62L^{hi}$). Increased frequencies and numbers of Tem were observed in all organs investigated but were most increased in lungs with a peak at days 8 – 20 *post* infection (Figures 2E–H; Figure 3 in Supplementary Material). Tem populations in MLNs were significantly increased at 8 dpi and remained increased until 29 dpi (Figures 2E, G). In spleen, Tem populations did not increase until days 20 and 29 *post* infection (Figures 2F, H). In ILNs, frequencies of both $CD4^+$ and $CD8^+$ Tem were elevated at 8 dpi and remained increased until 29 dpi (Figures 2F, H). At 3 dpi $CD4^+$ Tem and at 5 dpi $CD8^+$ Tem were increased in MesLNs and remained elevated until 29 dpi (Figures 2F, H). At seven months *post* infection the frequencies of $CD4^+$ Tem were higher than at baseline in all organs studied (Figures 2E, F). Frequencies of $CD8^+$ Tem were increased in all organs apart from MesLNs at seven months *post* infection (Figures 2G, H). Antigen-specific Tem significantly increased in all organs at 8 – 12 dpi with $M_{2\text{-}17}{}^+$ $CD4^+$ Tem being less abundant than $NP_{147\text{-}155}{}^+$ $CD8^+$ Tem (Figures 2I–L). In MesLNs a significant increase of $NP_{147\text{-}155}{}^+$ $CD8^+$ Tem was detected only at 8 dpi (Figure 2L). Numbers of $M_{2\text{-}17}{}^+$ $CD4^+$ Tem increased approximately 10 – 100 times in all organs studied 8 – 29 dpi (Figures 2M, N). The numbers of $NP_{147\text{-}155}{}^+$ $CD8^+$ Tem increased in MLNs, lungs, spleen and MesLNs at 8 dpi and remained in similar numbers in MLNs, spleen and MesLNs until 29 dpi whereas the numbers decreased in lungs (Figures 2O, P). At seven months *post* infection frequencies and numbers of $M_{2\text{-}17}{}^+$ $CD4^+$ Tem were increased in MLNs and ILNs whereas only the number of $M_{2\text{-}17}{}^+$ $CD4^+$ Tem was increased in spleen (Figures 2M, N). Increased numbers of $NP_{147\text{-}155}{}^+$ $CD8^+$ Tem were observed in lungs and in spleen at seven months *post* infection (Figures 2O, P). Collectively, the results are in agreement with previously published data that antigen-specific memory T cells are generated in organs directly involved in the infection. In this study, antigen-specific T cells were also detected in peripheral lymphoid organs distant from the site of viral replication. Furthermore, our data demonstrates long-term presence of antigen-specific Tem in MLN, lungs, spleen and ILNs when analyzed at seven months *post* infection.

Lung-resident $CD4^+CD69^+CD11a^+$ T cells increase in lung tissue after influenza virus infection

Apart from being a marker of activation, CD69 is a hallmark marker for Trm. Since an increase of CD69-expressing T cells was observed in lungs starting at 8 dpi we hypothesized that it was due to development of Trm in the lungs. In addition to CD69, $CD4^+$ Trm are defined by their expression of integrin CD11a (26, 35, 36). To verify that $CD4^+CD69^+CD11a^+$ T cells were localized to the lung tissue and not intravascularly, FITC-conjugated antibodies against the alloantigen CD45.2, present on the majority of hematopoietic cells, were injected intravenously three minutes prior to euthanasia. Indeed, >98% of the $CD4^+CD69^+CD11a^+$ T cells were protected from staining and therefore localized in the lung tissue (Figure 3A). In naïve mice, $CD4^+CD69^+CD11a^+$ T cells were scarce but from 3 dpi the frequency was significantly increased with a peak in numbers by day 8 *post* infection (Figures 3B, C). The frequency and number of influenza virus-specific $CD4^+$ $CD69^+CD11a^+$ T cells was increased from 8 dpi until 12 – 20 dpi, and at 210 dpi the

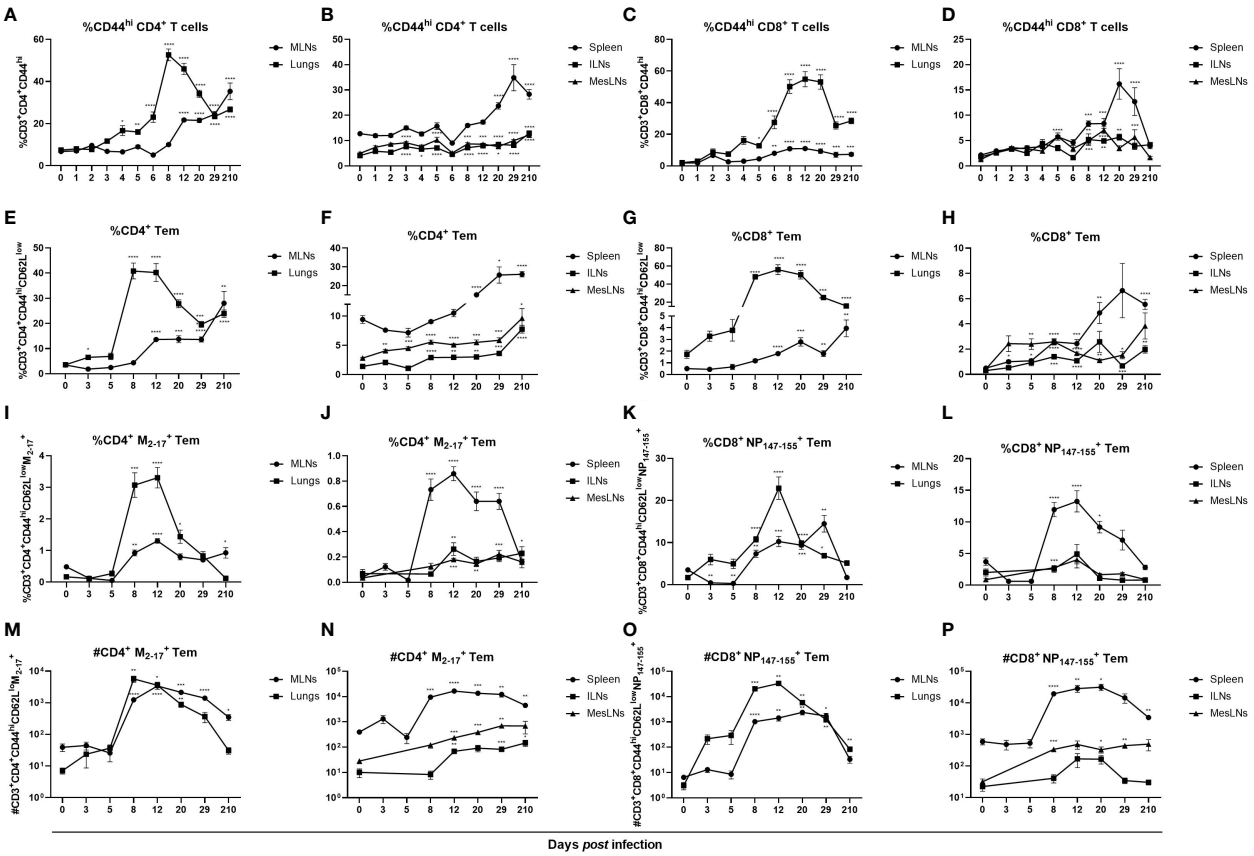

FIGURE 2
Influenza virus infection induced antigen-specific $CD4^+$ and $CD8^+$ Tem locally and systemically. Cells were stained with anti-CD44 antibodies to investigate the differentiation of effector T cells. $CD44^{hi}$ cells gated on $CD3^+CD4^+$ or $CD3^+CD8^+$ T cells in MLNs, lungs **(A, C)**, spleen, ILNs and MesLNs **(B, D)**. To separate $CD44^{hi}CD62L^{low}$ Tem from $CD44^{hi}CD62L^{hi}$ central memory T cells in MLNs, lungs **(E, G)**, spleen, ILNs and MesLNs **(F, H)** antibodies against the L-selectin CD62L was added to the flow cytometry panel. Frequencies of antigen-specific Tem were determined by staining with class II MHC tetramer M_{2-17} **(I, J)** and class I MHC tetramer $NP_{147-155}$ **(K, L)**. Numbers of antigen-specific $CD4^+$ Tem **(M, N)** and antigen-specific $CD8^+$ Tem **(O, P)**. Data in figures A – D are composites of 1 – 4 separate experiments per time point with 3 – 10 mice per group. Data in figures E – P are composites of 2 – 3 separate experiments per time point with 4 – 10 mice per group. Data are shown as mean ± SEM. *p < 0.05, **p < 0.01, ***p < 0.001 and ****p < 0.0001.

number of antigen-specific $CD4^+CD69^+CD11a^+$ T cells remained increased (Figure 3D). Thus, influenza virus infection results in the development of antigen-specific, lung-resident $CD4^+CD69^+CD11a^+$ T cells that persist at least seven months after infection.

$CD8^+CD103^-CD49a^+$ and $CD8^+CD103^+CD49a^+$ lung-resident T cells dominate at different stages in lung tissue during and after influenza virus infection

Based on the proposed location of the $CD8^+$ Trm subsets (Figure 4A) we sought to determine if differences in abundance of the different subsets could be observed at different time points after primary influenza virus infection (28). First it was verified that all three $CD8^+$ subsets mainly resided in the lung tissue and not in the pulmonary vasculature (Figure 4B). Naïve mice had few lung-resident T cells and only a minor increase in numbers was observed until 8 dpi, coinciding with the maximum weight loss (Figure 1A), when the $CD8^+CD103^-CD49a^+$ T cell subset dominated (Figures 4C–F). At 12 dpi the relative abundance of $CD8^+CD103^-CD49a^+$ T cells was similar to that of $CD8^+CD103^+CD49a^+$ T cells though slightly lower. $CD8^+CD103^+CD49a^+$ T cells were detected at 8 dpi and peaked in numbers at 12 dpi i.e. after the influenza virus is cleared, and was the main subset at 29 dpi (Figures 4C–F). At seven months *post* infection, the frequency of $CD8^+CD103^-CD49a^+$ T cells and numbers of all three lung-resident subsets remained increased (Figures 4C, D, F). $CD8^+CD103^+CD49a^-$ T cells appeared to play a minor role in the response against

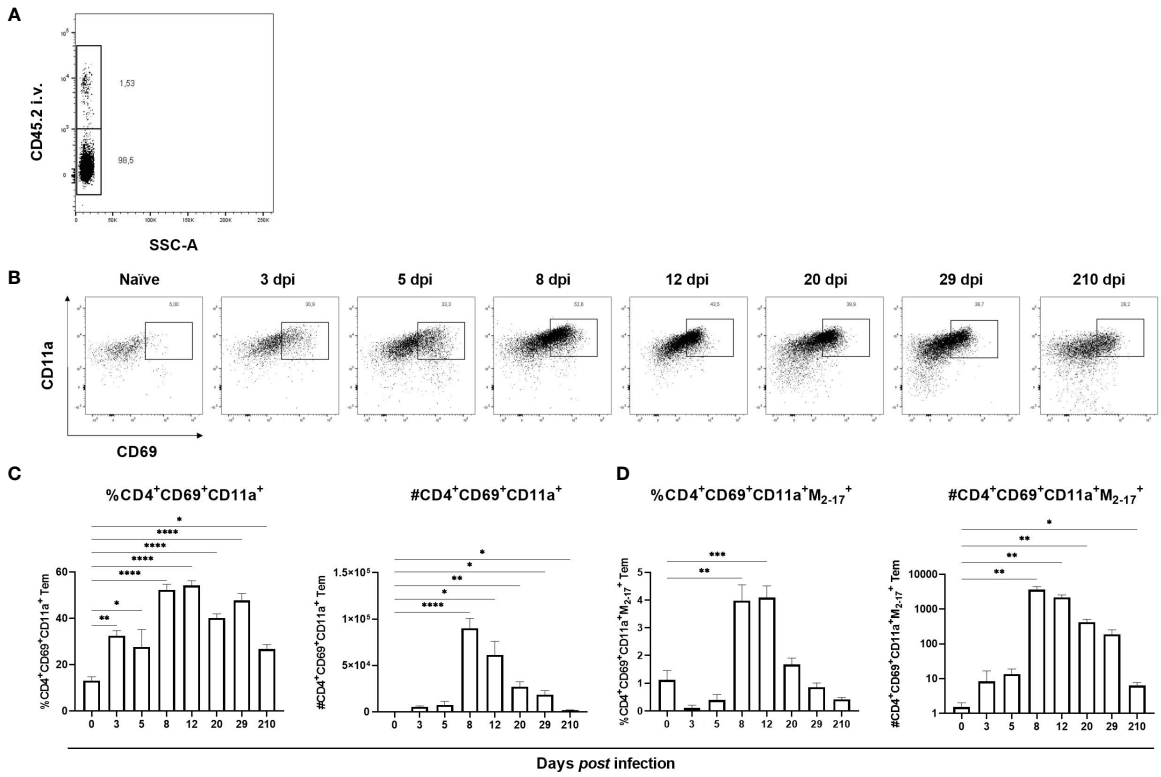

FIGURE 3
Formation of lung-resident CD4$^+$ T cells in lungs after influenza virus infection. CD4$^+$ Trm express CD69 and CD11a and to verify their localization to the lung tissue anti-CD45.2 antibodies were injected intravenously three minutes prior to euthanasia **(A)**. In **(B)** representative flow cytometry plots gated from CD4$^+$ Tem with up to 8000 events per plot from indicated time points after infection are shown. Frequency and numbers of lung-resident CD4$^+$CD69$^+$CD11a$^+$ T cells **(C)**. Frequency and numbers of antigen-specific, lung-resident CD4$^+$CD69$^+$CD11a$^+$ T cells **(D)**. Data are composites of two separate experiments with five mice per group. Data are shown as mean ± SEM. *p < 0.05, **p < 0.01, ***p < 0.001 and ****p < 0.0001.

influenza virus as this subset was represented by a low cell number and did not expand to the same extent as the other two subsets (Figures 4C–H). The number of antigen-specific CD8$^+$CD103$^+$CD49a$^+$ T cells remained increased until 7 months *post* infection, but the frequency varied substantially among mice due to low cell numbers and therefore the result should be interpreted with caution. In conclusion, CD8$^+$CD103$^-$CD49a$^+$ T cells are the dominating lung-resident CD8$^+$ subset at 8 dpi whereas CD8$^+$CD103$^+$CD49a$^+$ T cells become the most abundant subset after 12 dpi i.e. after the influenza virus has been cleared. Nevertheless, seven months after infection the frequencies of the two subsets are similar.

Discussion

To the best of our knowledge, this study is the first to describe the kinetics of the adaptive immune response in lymphoid organs peripheral to the respiratory tract and the emergence of different lung-resident CD8$^+$ T cell subsets during and after influenza virus infection. We studied the kinetics of the adaptive immune response by flow cytometry after infecting mice with PR8 intranasally and found that despite being an airway-restricted pathogen, influenza virus infection results in increased frequencies of activated B cells and T cells, and antigen-specific effector memory T cells in peripheral lymphoid organs, although to a minor extent than in tissues associated with the site of infection.

After entry, influenza virus replicates in airway-associated tissues, mainly in epithelial cells, which limits the infection to the respiratory tract. Viral antigens are taken up and transported by dendritic cells to draining MLNs within 48 hours *post* infection (13, 37–39). There, T cells recognizing cognate antigens presented on MHC by dendritic cells rapidly upregulate cell surface expression of CD69 resulting in downregulation of L-selectin and interference with sphingosine-1-phosphate receptor function to inhibit egress from the lymph node (40–42). Likewise, CD69 is upregulated on B cells shortly after activation (15). Thus, CD69 is suitable as an early activation

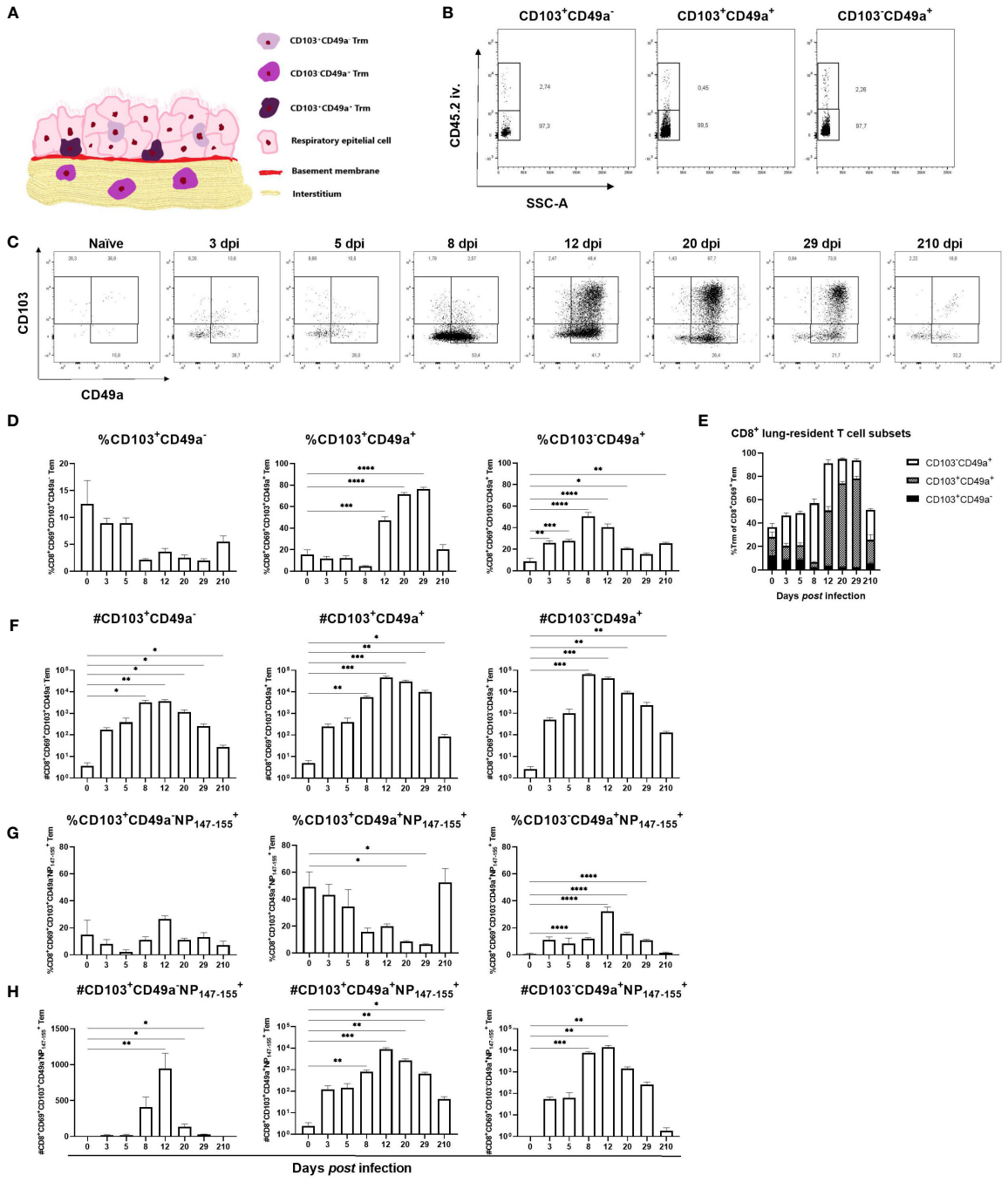

FIGURE 4
Kinetics of lung-resident CD8$^+$ T cell subsets in lungs after influenza virus infection. A modified illustration of the three subsets of CD8$^+$ Trm residing at different areas in the lungs as proposed in (28) **(A)**. Intravascular staining to confirm the localization of the three subsets of CD8$^+$ T cells in the lung tissue **(B)**. CD103$^+$CD49a$^-$, CD103$^-$CD49a$^+$ and CD103$^+$CD49a$^+$ T cell populations were gated from the CD8$^+$ Tem population. In **(C)**, representative flow cytometry plots from naïve mice and from influenza virus infected mice at indicated time points after infection displaying up to 8000 events. Proportion **(D)** and number **(F)** of each lung-resident CD8$^+$ T cell subset at indicated time points after PR8 infection. Numbers **(H)** and frequencies **(G)** of antigen-specific, lung-resident CD8$^+$ T cell subsets. In **(E)** a summary of the findings in **(D)** is shown. Data are composites of two separate experiments with 5 – 6 mice per group. Data are shown as mean ± SEM. *p < 0.05, **p < 0.01, ***p < 0.001 and ****p < 0.0001.

marker of B cells and T cells. The restricted site for virus replication was mirrored by the simultaneous early activation of B cells and T cells arguing for a similar time frame for binding of the differently processed antigenic forms to the antigen-binding receptors on the respective main lymphocyte population. In line with previous findings, the proportion of $CD19^+$ B cells increased in lungs from 8 dpi whereas activated $CD19^+$ B cells were increased at days three and eight but also at day 12 *post* infection in our study (33). In MLNs, a peak in activated $CD19^+$ B cells was detected at 3 dpi and taken together our results would be consistent with the findings that specific antibody-secreting B cells increase rapidly in MLNs only to drop close to baseline values 14 days after influenza-virus infection unlike in lungs where they increase starting from 7 dpi (43).

Although the activation of both helper T cells and cytotoxic T cells followed the same kinetic pattern in MLNs and lungs, their relative abundance was higher in lungs than in MLNs consistent with the lungs being the primary site of infection. We hypothesized that a peak of CD69-expressing T cells in MLNs would precede that of lungs since antigens are transported from lungs to MLNs to be presented to T cells followed by migration of activated, antigen-specific T cells from MLNs to lungs. In a skin infection model, infiltrating $CD8^+$ T cells, but not $CD4^+$ T cells, upregulate CD69 on their cell surfaces after skin entry which serves to retain the cells in the skin and later differentiate into resident memory T cells (41, 44). The increased frequencies of CD69-expressing T cells in lungs could be due to upregulation of CD69 by activated T cells migrating from MLNs and since CD69 is also associated with tissue-residency it would further argue for $CD69^+$ migratory MLN T cells as the main source of activated T cells in the lungs (40). An additional explanation would be homing of peripheral, naïve T cells to the site of infection as has been demonstrated in mice infected with the intestinal nematode *Heligmosomoides polygyrus* (14, 45, 46). We observed a transient decrease in ILN cellularity which indicates a redistribution of lymphocytes to expand the population at the site of infection as previously reported in influenza virus-infected mice as well as in *Heligmosomoides polygyrus* infected mice (14, 40, 46). Virus-specific memory T cells were primarily detected in lungs and lung-draining MLNs but also in peripheral lymphoid organs not targeted by the infection. Presence of viral RNA with subsequent activation and generation of memory T cells has been observed previously in spleen after influenza virus infection but not in peripheral ILNs, MesLNs, axillary lymph nodes or brachial lymph nodes (14). Whether the increase of antigen-specific Tem in ILNs and MesLNs is due to antigen-presentation by migratory DCs from the site of infection in the same manner as in spleen or is due to migration of differentiated Tem from MLNs remains to be investigated (14, 40).

In this study, we confirmed that influenza virus infection generates lung-resident memory $CD4^+$ and $CD8^+$ T cells which are reported to be crucial for conveying homologous and heterosubtypic immunity that mediate a fast local protection already within 24 hours after homologous infection and by clearing the heterologous virus 36 – 48 hours faster in immune mice than in primary infected mice (18, 47, 48). Various surface markers have been identified as expressed by different subsets of tissue-resident memory T cells with CD69 as a canonical marker (29, 47, 49, 50). Expression of CD49a but not CD103 has proven to be essential for Trm to confer heterosubtypic immunity and for the cells' ability to migrate in the tissue whereas CD103 limits migration by reducing the cells' velocity (51). $CD8^+CD103^-CD49a^+$ T cells expanded and was the major subset at 8 dpi coinciding with the time point when the virus is cleared (3, 33, 48) and clinical signs of infection, i.e. weight loss, are most pronounced. The ability to migrate in infected tissues is an important feature of cells involved in pathogen clearance which would support that $CD8^+CD103^-CD49a^+$ T cells is the dominant subset initially as they do not express the speed-limiting CD103. Mice develop interstitial pneumonia after influenza virus infection and given their proposed location in the lung tissue and their effector functions as supreme perforin producers, $CD8^+CD103^-CD49a^+$ T cells may expand to combat the infection as an effector subset rather than a memory cell subset (28, 29, 52). In influenza virus-immune mice treated with FTY720 and challenged with a heterologous virus mainly $CD103^-$ tissue-resident $CD4^+$ and $CD8^+$ T cells conferred protective immunity indicating a possible effector role of $CD8^+CD103^-CD49a^+$ T cells (27). However, CD49a-expression was not included in that study. Nevertheless, $CD8^+CD103^+CD49a^+$ T cells exert similar antiviral effector functions as $CD8^+CD103^-CD49a^+$ T cells but is the dominating subset after clearance of infection indicating a more profound memory cell phenotype and may function as sensors for new infections since immune cells in the interstitium are scarce in naïve lungs (53, 54). After cutaneous herpes simplex infection, the majority of Trm in the skin express CD49a at 7 – 9 dpi whereas at 16 dpi Trm co-express CD103 and CD49a, a phenotype that dominates in the memory phase (55). The localization of eTrm would allow them to surveil both the interstitium and epithelial cells for viral antigens enabling them to perform immunosurveillance and protect the tissue from future influenza virus infections. Thus, the presence of influenza virus-specific lung-resident T cells in the lung up to 7 months post infection is in support of such a hypothesis. Whether $CD8^+CD103^-CD49a^+$ T cells differentiate into $CD8^+CD103^+CD49a^+$ T cells by migrating to the basal respiratory epithelium and upregulate cell surface expression of CD103 or if the $CD8^+CD103^+CD49a^+$ T cells develop as a separate subset remains to be investigated. In the current study, the $CD8^+CD103^+CD49a^-$ T cells did not expand to the same extent as $CD8^+CD103^-CD49a^+$ T cells and $CD8^+CD103^+CD49a^+$ T cells subsets and therefore may play a minor role, if any, during influenza virus infection in mice, a theory supported by the fact that $CD103^+$ Trm do not remain three months after influenza virus infection and phenotypically resemble circulating memory T cells (29).

The intranasal infection with the H1N1 influenza A virus constitutes a highly relevant model for the study of the adaptive

immune response to emerging respiratory viruses including the early kinetics of differentiation of recruited, antigen-specific T cells. The results presented here increase the existing knowledge of adaptive immune responses to influenza virus infection, mapping the kinetics of tissue T cell memory expansion and contraction. In addition, we have demonstrated that two $CD8^+$ lung-resident T cell subsets vary in abundance at different stages after influenza virus infection, a finding that can be further investigated in coming studies focusing on the origin, regulation, roles and functions of the respective subsets. Induction of memory T cells against heterologous influenza virus can protect the host against pandemic strains but also yields a better protection against new seasonal strains. A better understanding of the developmental steps in the kinetics of the T cell response, including Trm, would enhance the knowledge about T cell biology and aid in the generation of vaccines against respiratory viruses, in particular by targeting Trm generation and their maintenance.

Data availability statement

The original contributions presented in the study are included in the article/Supplementary Material. Further inquiries can be directed to the corresponding author.

Ethics statement

The animal study was reviewed and approved by the regional animal ethics committee of Uppsala, Sweden.

Author contributions

ME and K-OG designed the study, wrote the manuscript, collected data and interpreted the results. ME performed the *in vivo* experiments, performed the data analysis and prepared the figures. ME, SN and K-OG reviewed, discussed and approved the final version of the manuscript. All authors contributed to the article and approved the submitted version.

Funding

This work was funded by the National Veterinary Institute and Uppsala Immunobiology Lab. The National Veterinary Institute funded ME, the animal studies and reagents. Uppsala Immunobiology Lab funded reagents and the research lab. SN and publishing cost were supported by Karolinska Institute intramural funds.

Acknowledgments

We thank the NIH Tetramer Core Facility (contract number 75N93020D00005) for providing the tetramers.

Conflict of interest

The authors declare that the research was conducted in the absence of any commercial or financial relationships that could be construed as a potential conflict of interest.

Publisher's note

Supplementary material

The Supplementary Material for this article can be found online at: https://www.frontiersin.org/articles/10.3389/fimmu.2022.949299/full#supplementary-material

References

1. Iuliano AD, Roguski KM, Chang HH, Muscatello DJ, Palekar R, Tempia S, et al. Estimates of global seasonal influenza-associated respiratory mortality: a modelling study. *Lancet (London England).* (2018) 391(10127):1285–300. doi: 10.1016/S0140-6736(17)33293-2

2. Czakó R, Vogel L, Lamirande EW, Bock KW, Moore IN, Ellebedy AH, et al. Vivo imaging of influenza virus infection in immunized mice. *mBio* (2017) 8(3): e00714–17. doi: 10.1128/mBio.00714-17

3. Kim JH, Bryant H, Fiedler E, Cao T, Rayner JO. Real-time tracking of bioluminescent influenza a virus infection in mice. *Sci Rep* (2022) 12(1):3152. doi: 10.1038/s41598-022-06667-w

4. Ibricevic A, Pekosz A, Walter MJ, Newby C, Battaile JT, Brown EG, et al. Influenza virus receptor specificity and cell tropism in mouse and human airway epithelial cells. *J Virol* (2006) 80(15):7469–80. doi: 10.1128/JVI.02677-05

5. Luo M. Influenza virus entry. *Adv Exp Med Biol* (2012) 726:201–21. doi: 10.1007/978-1-4614-0980-9_9

6. Inaba K, Turley S, Yamaide F, Iyoda T, Mahnke K, Inaba M, et al. Efficient presentation of phagocytosed cellular fragments on the major histocompatibility complex class II products of dendritic cells. *J Exp Med* (1998) 188(11):2163–73. doi: 10.1084/jem.188.11.2163

7. Albert ML, Sauter B, Bhardwaj N. Dendritic cells acquire antigen from apoptotic cells and induce class I-restricted CTLs. *Nature.* (1998) 392(6671):86–9. doi: 10.1038/32183

8. Bender A, Albert M, Reddy A, Feldman M, Sauter B, Kaplan G, et al. The distinctive features of influenza virus infection of dendritic cells. *Immunobiology.* (1998) 198(5):552–67. doi: 10.1016/S0171-2985(98)80078-8

9. Bohineust A, Garcia Z, Beuneu H, Lemaître F, Bousso P. Termination of T cell priming relies on a phase of unresponsiveness promoting disengagement from APCs and T cell division. *J Exp Med* (2018) 215(5):1481–92. doi: 10.1084/jem.20171708

10. Mempel TR, Henrickson SE, von Andrian UH. T-Cell priming by dendritic cells in lymph nodes occurs in three distinct phases. *Nature.* (2004) 427(6970):154–9. doi: 10.1038/nature02238

11. Kim TS, Braciale TJ. Respiratory dendritic cell subsets differ in their capacity to support the induction of virus-specific cytotoxic CD8+ T cell responses. *PloS One* (2009) 4(1):e4204. doi: 10.1371/journal.pone.0004204

12. Hamilton-Easton A, Eichelberger M. Virus-specific antigen presentation by different subsets of cells from lung and mediastinal lymph node tissues of influenza virus-infected mice. *J Virol* (1995) 69(10):6359–66. doi: 10.1128/jvi.69.10.6359-6366.1995

13. Moltedo B, Li W, Yount JS, Moran TM. Unique type I interferon responses determine the functional fate of migratory lung dendritic cells during influenza virus infection. *PloS pathogens.* (2011) 7(11):e1002345. doi: 10.1371/journal.ppat.1002345

14. Turner DL, Bickham KL, Farber DL, Lefrancois L. Splenic priming of virus-specific CD8 T cells following influenza virus infection. *J Virol* (2013) 87(8):4496–506. doi: 10.1128/JVI.03413-12

15. Hara T, Jung LK, Bjorndahl JM, Fu SM. Human T cell activation III. rapid induction of a phosphorylated 28 kD/32 kD disulfide-linked early activation antigen (EA 1) by 12-o-tetradecanoyl phorbol-13-acetate, mitogens, and antigens. *J Exp Med* (1986) 164(6):1988–2005. doi: 10.1084/jem.164.6.1988

16. Moretta A, Poggi A, Pende D, Tripodi G, Orengo AM, Pella N, et al. CD69-mediated pathway of lymphocyte activation: anti-CD69 monoclonal antibodies trigger the cytolytic activity of different lymphoid effector cells with the exception of cytolytic T lymphocytes expressing T cell receptor alpha/beta. *J Exp Med* (1991) 174(6):1393–8. doi: 10.1084/jem.174.6.1393

17. Testi R, Phillips JH, Lanier LL. Leu 23 induction as an early marker of functional CD3/T cell antigen receptor triggering. requirement for receptor cross-linking, prolonged elevation of intracellular [Ca++] and stimulation of protein kinase c. *J Immunol (Baltimore Md 1950).* (1989) 142(6):1854–60.

18. Liang S, Mozdzanowska K, Palladino G, Gerhard W. Heterosubtypic immunity to influenza type a virus in mice Effector mechanisms and their longevity. *J Immunol (Baltimore Md 1950).* (1994) 152(4):1653–61.

19. Sanders ME, Makgoba MW, Sharrow SO, Stephany D, Springer TA, Young HA, et al. Human memory T lymphocytes express increased levels of three cell adhesion molecules (LFA-3, CD2, and LFA-1) and three other molecules (UCHL1, CDw29, and pgp-1) and have enhanced IFN-gamma production. *J Immunol* (1988) 140(5):1401–7.

20. DeGrendele HC, Kosfiszer M, Estess P, Siegelman MH. CD44 activation and associated primary adhesion is inducible *via* T cell receptor stimulation. *J Immunol* (1997) 159(6):2549–53.

21. Gerlach C, Moseman EA, Loughhead SM, Alvarez D, Zwijnenburg AJ, Waanders L, et al. The chemokine receptor CX3CR1 defines three antigen-experienced CD8 T cell subsets with distinct roles in immune surveillance and homeostasis. *Immunity.* (2016) 45(6):1270–84. doi: 10.1016/j.immuni.2016.10.018

22. Hogan RJ, Usherwood EJ, Zhong W, Roberts AD, Dutton RW, Harmsen AG, et al. Activated antigen-activated antigen-specific CD8+ T cells persist in the lungs following recovery from respiratory virus infections. *J Immunol* (2001) 166 (3):1813–22. doi: 10.4049/jimmunol.166.3.1813

23. Budd RC, Cerottini JC, Horvath C, Bron C, Pedrazzini T, Howe RC, et al. Distinction of virgin and memory T lymphocytes Stable acquisition of the pgp-1 glycoprotein concomitant with antigenic stimulation. *J Immunol (Baltimore Md 1950).* (1987) 138(10):3120–9.

24. Cheuk S, Schlums H, Gallais Sérézal I, Martini E, Chiang SC, Marquardt N, et al. CD49a expression defines tissue-resident CD8(+) T cells poised for cytotoxic function in human skin. *Immunity.* (2017) 46(2):287–300. doi: 10.1016/j.immuni.2017.01.009

25. Kumar BV, Ma W, Miron M, Granot T, Guyer RS, Carpenter DJ, et al. Human tissue-resident memory T cells are defined by core transcriptional and functional signatures in lymphoid and mucosal sites. *Cell Rep* (2017) 20(12):2921–34. doi: 10.1016/j.celrep.2017.08.078

26. Teijaro J, Turner D, Pham Q-M, Wherry EJ, Lefrançois L, Farber D. Cutting edge: Tissue-retentive lung memory CD4 T cells mediate optimal protection to respiratory virus infection. *J Immunol (Baltimore Md 1950).* (2011) 187:5510–4. doi: 10.4049/jimmunol.1102243

27. Paik DH, Farber DL. Influenza infection fortifies local lymph nodes to promote lung-resident heterosubtypic immunity. *J Exp Med* (2021) 218(1): e20200218. doi: 10.1084/jem.20200218

28. Topham DJ, Reilly EC, Emo KL, Sportiello M. Formation and maintenance of tissue resident memory CD8+ T cells after viral infection. *Pathog (Basel Switzerland).* (2019) 8(4):196. doi: 10.3390/pathogens8040196

29. Reilly EC, Sportiello M, Emo KL, Amitrano AM, Jha R, Kumar ABR, et al. CD49a identifies polyfunctional memory CD8 T cell subsets that persist in the lungs after influenza infection. *Front Immunol* (2021) 12(3679). doi: 10.3389/fimmu.2021.728669

30. Ashman RB. Persistence of cell-mediated immunity to influenza a virus in mice. *Immunology.* (1982) 47(1):165–8.

31. Wallach MG, Webby RJ, Islam F, Walkden-Brown S, Emmoth E, Feinstein R, et al. Cross-protection of chicken immunoglobulin y antibodies against H5N1 and H1N1 viruses passively administered in mice. *Clin Vaccine Immunol* (2011) 18 (7):1083–90. doi: 10.1128/CVI.05075-11

32. Anderson KG, Mayer-Barber K, Sung H, Beura L, James BR, Taylor JJ, et al. Intravascular staining for discrimination of vascular and tissue leukocytes. *Nat Protoc* (2014) 9(1):209–22. doi: 10.1038/nprot.2014.005

33. Toapanta FR, Ross TM. Impaired immune responses in the lungs of aged mice following influenza infection. *Respir Res* (2009) 10:112. doi: 10.1186/1465-9921-10-112

34. Pociask DA, Robinson KM, Chen K, McHugh KJ, Clay ME, Huang GT, et al. Epigenetic and transcriptomic regulation of lung repair during recovery from influenza infection. *Am J pathology.* (2017) 187(4):851–63. doi: 10.1016/j.ajpath.2016.12.012

35. Turner DL, Bickham KL, Thome JJ, Kim CY, D'Ovidio F, Wherry EJ, et al. Lung niches for the generation and maintenance of tissue-resident memory T cells. *Mucosal Immunol* (2014) 7(3):501–10. doi: 10.1038/mi.2013.67

36. Turner DL, Farber DL. Mucosal resident memory CD4 T cells in protection and immunopathology. *Front Immunol* (2014) 5:331–. doi: 10.3389/fimmu.2014.00331

37. Ho AW, Prabhu N, Betts RJ, Ge MQ, Dai X, Hutchinson PE, et al. Lung CD103+ dendritic cells efficiently transport influenza virus to the lymph node and load viral antigen onto MHC class I for presentation to CD8 T cells. *J Immunol (Baltimore Md 1950).* (2011) 187(11):6011–21. doi: 10.4049/jimmunol.1100987

38. Allenspach EJ, Lemos MP, Porrett PM, Turka LA, Laufer TM. Migratory and lymphoid-resident dendritic cells cooperate to efficiently prime naive CD4 T cells. *Immunity.* (2008) 29(5):795–806. doi: 10.1016/j.immuni.2008.08.013

39. Eichelberger MC, Wang ML, Allan W, Webster RG, Doherty PC. Influenza virus RNA in the lung and lymphoid tissue of immunologically intact and CD4-depleted mice. *J Gen virology.* (1991) 72(Pt 7):1695–8. doi: 10.1099/0022-1317-72-7-1695

40. Lawrence CW, Braciale TJ. Activation, differentiation, and migration of naive virus-specific CD8+ T cells during pulmonary influenza virus infection. *J Immunol (Baltimore Md 1950).* (2004) 173(2):1209–18. doi: 10.4049/jimmunol.173.2.1209

41. Mackay LK, Braun A, Macleod BL, Collins N, Tebartz C, Bedoui S, et al. Cutting edge: CD69 interference with sphingosine-1-phosphate receptor function regulates peripheral T cell retention. *J Immunol (Baltimore Md 1950).* (2015) 194 (5):2059–63. doi: 10.4049/jimmunol.1402256

42. Bankovich AJ, Shiow LR, Cyster JG. CD69 suppresses sphingosine 1-phosophate receptor-1 (S1P1) function through interaction with membrane helix 4. *J Biol Chem* (2010) 285(29):22328–37. doi: 10.1074/jbc.M110.123299

43. Rothaeusler K, Baumgarth N. B-cell fate decisions following influenza virus infection. *Eur J Immunol* (2010) 40(2):366–77. doi: 10.1002/eji.200939798

44. Jaigirdar SA, Benson RA, Elmesmari A, Kurowska-Stolarska MS, McInnes IB, Garside P, et al. Sphingosine-1-Phosphate promotes the persistence of activated CD4 T cells in inflamed sites. *Front Immunol* (2017) 8. doi: 10.3389/fimmu.2017.01627

45. Feng X, Classon C, Terán G, Yang Y, Li L, Chan S, et al. Atrophy of skin-draining lymph nodes predisposes for impaired immune responses to secondary infection in mice with chronic intestinal nematode infection. *PloS pathogens.* (2018) 14(5):e1007008. doi: 10.1371/journal.ppat.1007008

46. King IL, Mohrs K, Meli AP, Downey J, Lanthier P, Tzelepis F, et al. Intestinal helminth infection impacts the systemic distribution and function of the naive lymphocyte pool. *Mucosal Immunol* (2017) 10(5):1160–8. doi: 10.1038/mi.2016.127

47. Gilchuk P, Hill TM, Guy C, McMaster SR, Boyd KL, Rabacal WA, et al. A distinct lung-Interstitium-Resident memory CD8(+) T cell subset confers enhanced protection to lower respiratory tract infection. *Cell Rep* (2016) 16 (7):1800–9. doi: 10.1016/j.celrep.2016.07.037

48. Dutta A, Huang CT, Lin CY, Chen TC, Lin YC, Chang CS, et al. Sterilizing immunity to influenza virus infection requires local antigen-specific T cell response in the lungs. *Sci Rep* (2016) 6:32973. doi: 10.1038/srep32973

49. Galvez-Cancino F, Lopez E, Lladser A. Analysis of tissue-resident immune cells from mouse skin and lungs by flow cytometry. *Methods Protoc* (2019) 19132019:217–22. doi: 10.1007/978-1-4939-8979-9_16

50. Topham DJ , Reilly EC. Tissue-resident memory CD8(+) T cells: From phenotype to function. *Front Immunol* (2018) 9:515. doi: 10.3389/fimmu.2018.00515

51. Reilly EC, Lambert Emo K, Buckley PM, Reilly NS, Smith I, Chaves FA, et al. TRM integrins CD103 and CD49a differentially support adherence and motility after resolution of influenza virus infection. *Proc Natl Acad Sci United States America.* (2020) 117(22):12306–14. doi: 10.1073/pnas.1915681117

52. Fukushi M, Ito T, Oka T, Kitazawa T, Miyoshi-Akiyama T, Kirikae T, et al. Serial histopathological examination of the lungs of mice infected with influenza a virus PR8 strain. *PloS One* (2011) 6(6):e21207–e. doi: 10.1371/journal.pone.0021207

53. Schenkel JM, Fraser KA, Vezys V, Masopust D. Sensing and alarm function of resident memory CD8$^+$ T cells. *Nat Immunol* (2013) 14(5):509–13. doi: 10.1038/ni.2568

54. Barletta KE, Cagnina RE, Wallace KL, Ramos SI, Mehrad B, Linden J. Leukocyte compartments in the mouse lung: distinguishing between marginated, interstitial, and alveolar cells in response to injury. *J Immunol Methods* (2012) 375 (1-2):100–10. doi: 10.1016/j.jim.2011.09.013

55. Bromley SK, Akbaba H, Mani V, Mora-Buch R, Chasse AY, Sama A, et al. CD49a regulates cutaneous resident memory CD8(+) T cell persistence and response. *Cell Rep* (2020) 32(9):108085. doi: 10.1016/j.celrep.2020.108085